Orbital analysis of electronic structure and phonon dispersion in MoS_2, $MoSe_2$, WS_2, and WSe_2 monolayers under strain

Chung-Huai Chang
Department of Physics, National Taiwan University, Taipei, Taiwan
and Institute of Atomic and Molecular Sciences, Academia Sinica, Taipei, Taiwan

Xiaofeng Fan
College of Materials Science and Engineering, Jilin University, Changchun, China

Shi-Hsin Lin* and Jer-Lai Kuo†
Institute of Atomic and Molecular Sciences, Academia Sinica, Taipei, Taiwan

(Received 22 August 2013; revised manuscript received 18 October 2013; published 19 November 2013)

Structures, electronic properties, and phonon dispersions of monolayer MX_2 (M = Mo, W; X = S, Se) under various types of mechanical strains are investigated with density functional calculations. By analyzing the orbitals near band gaps, we demonstrate that the X-M-X bond angle, together with the X-X distances, plays one of the most important roles in determining band gaps, as it is directly related to the coupling of d orbitals of the M atoms and p orbitals of the X atoms. It is found that the band gaps of monolayer MX_2 are more sensitive to biaxial strains. This notion can be attributed to the fact that, under biaxial strains, MX_2 tends to be stretched more significantly along the out-of-plane direction, resulting in greater changes in bond lengths/angles than uniaxial strains. While most theoretical reports suggested systematic reduction of band gaps under mechanical strains, we found that the direct band gaps can be robustly widened by applying compressive biaxial strains. Our results are of immediate importance for the recent experimental advances in applying compressive strains, which was not applicable before. On the other hand, the anisotropy of X-M-X bond angles induced by uniaxial strains leads to splitting in the phonon dispersion, and is directly relevant to recent Raman spectroscopy results. As most transition-metal dichalcogenides share the same structural characters, we expect that the notions derived here are applicable to other layered transition-metal oxides/chalcogenides and open up new venues to engineer their properties.

DOI: 10.1103/PhysRevB.88.195420 PACS number(s): 73.90.+f, 73.22.Pr

I. INTRODUCTION

Two-dimensional (2D) materials have been a hot research area since the novel and easy fabrication method "micromechanical cleavage" was introduced by Novoselov and Geim. Following the success of graphene, several stable 2D and quasi-2D materials with high-crystal qualities, such as BN, transition-metal dichalcogenides (TMDCs, such as MoS_2), and a few other layered complex oxides, have also been synthesized under ambient pressure.[1] There is no doubt that graphene is the most widely studied 2D material because of its unique and fascinating electronic properties.[2] However, the gapless feature of pristine graphene limits its applications on microelectronic devices.[3]

On the other hand, TMDCs are semiconductors, long known for their numerous applications in lubrication,[4] catalysis,[5] photoelectrochemical cells,[6] and photodetection.[7] As the rise of 2D materials, TMDCs received renewed attention, owing to their layered structures resembling graphite. They consist of stacked quasi-2D layers of MX_2 (M, transition-metal atom; X, chalcogen atom). Monolayers and few layers of MX_2 can now be fabricated and show promising electronic properties.[8] For example, it was recently shown that the gaps of many monolayer MX_2 are direct[9–11] with strong photoluminescence.[9,12,13]

Due to its importance for optoelectronics, the characteristics of band gaps were extensively investigated in the past. In 2010, Heinz's group experimentally demonstrated that a monolayer MoS_2 is a direct gap semiconductor with a band gap of 1.9 eV, whereas bulk MoS_2 has an indirect gap of 1.3 eV.[9,14] Several theoretical studies soon examined the electronic properties of the monolayer and few-layer TMDCs (Refs. 10 and 11) and found the gaps of monolayer MX_2 (M = Mo, W; X = S, Se, Te) in the range of 1.1 to 1.9 eV, suggesting that many TMDCs are strong candidates for optoelectronic applications. Furthermore, for a wider range of applications, it is very important to explore the tunability of band gaps. Applying mechanical strains is one of the most promising routes to manipulate band gaps of these quasi-2D materials and facilitate applications such as field effect transistors.[15] In addition, a few theoretical groups reported a systematic reduction of band gaps under mechanical strains.[16–21] Despite numerous theoretical efforts, there is a lack of a clear physical explanation behind the modification of electronic structures under strains.

In this work, we examine the change of band structures and phonon dispersions of monolayer of MX_2 (M = Mo, W; X = S, Se) under biaxial and uniaxial strains with first-principles calculations. The electronic states near the conduction minimum and valence band maximum are dominated by couplings of p orbitals of X atoms and d_{z^2}, $d_{x^2-y^2}$, and d_{xy} orbitals of M atoms. Therefore, the effectiveness of strains to modify the X-M-X bond angle largely determines the modulations of the band gaps. In general, the band gaps of monolayer MX_2 are more sensitive to the biaxial strains than the unaxial ones. In contrast to other theoretical reports, we carried out calculations

with finer grids of applied strains and found that it is possible to widen the direct gaps of MX_2 by applying compressive biaxial strains. Our results are of immediate importance for the recent experimental advances in applying compressive strains, which was not applicable before. On the other hand, the X-M-X bond angle can cause the splitting of phonon dispersions in the uniaxial cases, which is accessible with Raman spectroscopy. This paper is organized as follows: the computational method is detailed in Sec. II, and the contributions from different molecular orbitals to the band structures are analyzed in Sec. III. We demonstrate the modulations of band gaps and phonon modes under various strains, and propose an united mechanism in Secs. IV and V. Our conclusions are summarized in Sec. VI.

II. COMPUTATIONAL METHOD

The first-principles calculations were performed with the accurate frozen-core full-potential projector augmented-wave (PAW) method,[22,23] as implemented in the Vienna *ab initio* simulation package[24,25] (VASP). Several electron exchange-correlation functionals, including local density approximation (LDA), Perdew-Burke-Ernzerhof functional[26] (PBE), and PBE with dispersion[27] (PBE-D), were engaged for our calculations. We adopted a plane-wave cutoff energy 460 eV and an $18 \times 18 \times 1$ k-point grid centered at the Γ point. In addition, a 20-Å vacuum spacing was adopted to prevent artificial couplings between adjacent layers in the periodic supercells. The convergence criterion for the self-consistent field energy was set to be 10^{-6} eV and the Hellmann-Feynman forces acting on each atom were less than 0.01 eV/Å for each ionic step. The force constant (Hessian matrix) was calculated with density functional perturbation theory using VASP, and phonon dispersions were then obtained by diagonalizing the dynamical matrix.[28]

The structures of monolayer MX_2 (M = Mo, W; X = S, Se) are hexagonal lattices. In each unit cell, the M atom is

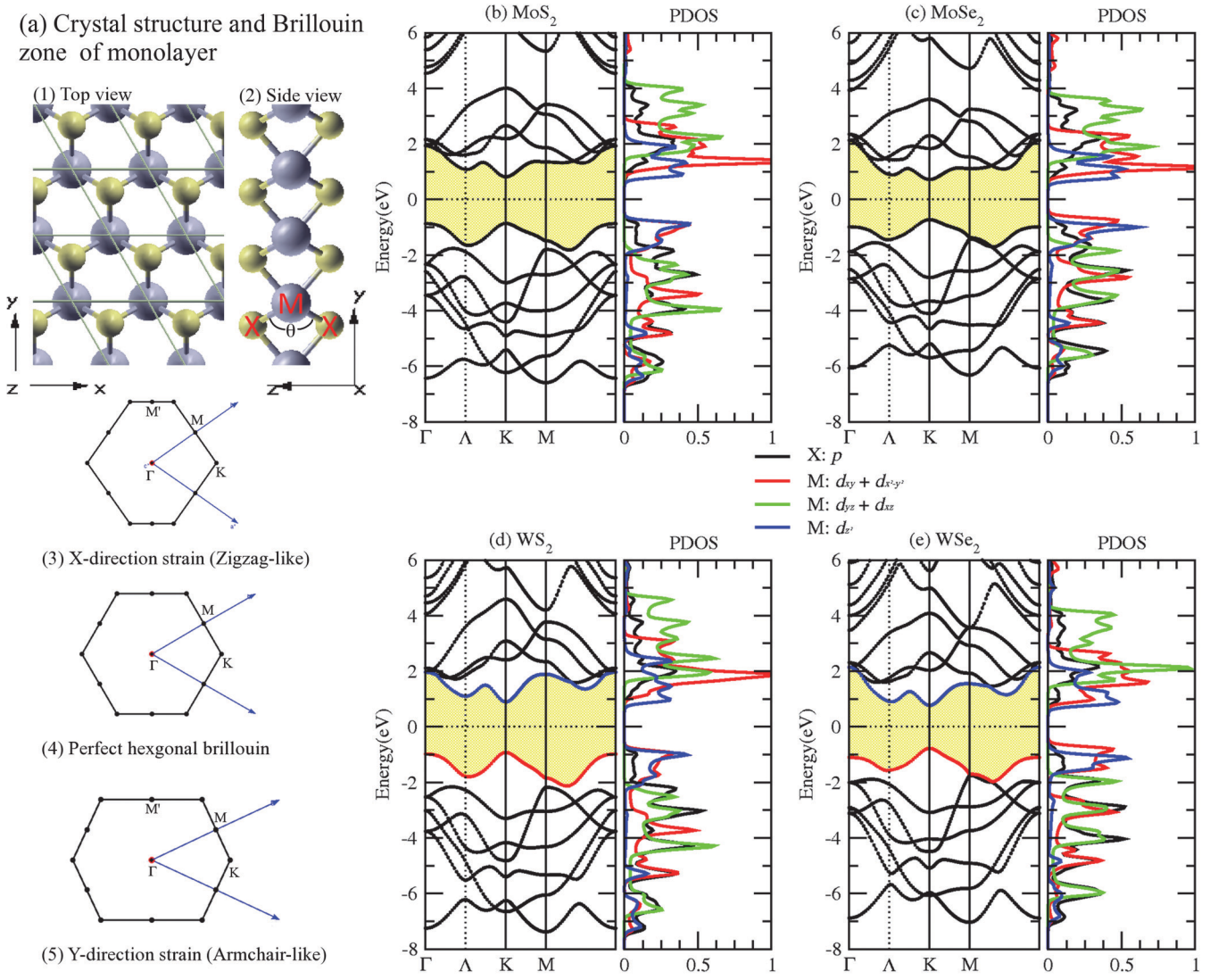

FIG. 1. (Color online) The top and side views of the 2D honeycomb crystal structure of monolayer MX_2 are shown in (a-1) and (a-2), respectively. The unit cells of monolayers are changed under uniaxial tensile strain conditions, which results in the shrinking Brillouin zone [(a-3) and (a-5)]. The perfect hexagonal Brillouin zone (a-4) is also shown for comparison. The band structures and partial density of states of different molecular orbitals, under PBE, are presented.

TABLE I. Lattice parameters in Å and band gaps in eV of monolayer MX_2. E_g reported here are those of the direct band gap except those marked with a star (*). The experimental lattice constants (Ref. 18) and band gaps (Refs. 9, 29, and 30) are listed as expt. for comparison.

Material		a (Å)	d_{M-X} (Å)	d_{X-X} (Å)	θ_{M-X} (Å)	E_g (eV)
MoS_2	PBE	3.18	2.41	3.13	80.76	1.679
	LDA	3.12	2.38	3.11	81.64	1.866
	expt.	3.160				1.90
$MoSe_2$	PBE	3.32	2.54	3.34	82.11	1.444
	LDA	3.25	2.50	3.32	83.03	1.613*
	expt.	3.299				1.57
WS_2	PBE	3.18	2.42	3.14	81.01	1.819
	LDA	3.16	2.39	3.12	81.76	1.999
	expt.	3.155				1.94–1.99
WSe_2	PBE	3.32	2.55	3.35	82.43	1.548
	LDA	3.25	2.51	3.33	83.29	1.678*
	expt.	3.286				1.65

bonded to six neighboring X atoms to form a triangular prism [see Figs. 1(a-1) and 1(a-2)]. The lattice constants and key bond lengths/angles, calculated with GGA-PBE and LDA, are complied in Table I. We also examined the role of the dispersion force and found that the difference between PBE and PBE-D is less than 0.3%. We should point out that while the dispersion correction plays a minor role on the structure of the monolayer MX_2, it is expected to be critical for the structure and properties of multilayer and bulk MX_2.

From Table I, it is found that the lattice constants calculated by PBE are generally longer than those by LDA (the deviations are roughly 2.0%, 2.3%, 1.8%, and 2.2% for MoS_2, $MoSe_2$, WS_2, and WSe_2, respectively). The bond lengths of M-X calculated by PBE reveal the same trend (the deviations are 1.3%, 1.6%, 1.3%, and 1.5%, respectively). However, it is interesting to find that the nonbonding distances between the two X atoms calculated by PBE and LDA are very close (the deviations are 0.4%, 0.6%, 0.5%, and 0.6%, respectively). This implies that the bond angles of X-M-X [see Fig. 1(a-2)] calculated by LDA is systematically larger than that by PBE calculations. The differences between the electronic structures obtained with LDA and PBE will be further discussed in the next section.

To simulate these quasi-2D materials under biaxial strains, the hexagonal unit cell is enlarged or shrunk with specific ratios, meanwhile allowing all the atomic positions to relax. In this way, the shape of the Brillouin zone retains the perfect hexagon symmetry and only sizes are varied [in Fig. 1(a-4)]. Uniaxial strains can be applied along two distinct directions of the hexagonal lattice. Following the conventions of graphene, the tensile strain in the zigzag direction is labeled as the x direction and the armchair direction as the y direction [shown in Fig. 1(a-1)]. When applying either zigzaglike or armchairlike strain, the unit cell of these quasi-2D systems is no longer an equilateral triangular lattice. This leads to an imperfect hexagonal Brillouin zone as shown in Figs. 1(a-3) and 1(a-5). The symmetric property of some k points, such as M and M', is broken and this implies that the band structures on some high-symmetry lines, such as Γ-M and Γ-M', are different. The area of the monolayer is kept fixed for the uniaxial strains in this work. This is because we found that conservation of the area typically leads to the most stable form. This notion is validated up to 5.3% strain along the armchair direction and 6.1% strain along the zigzag direction for all candidate materials.

III. BAND STRUCTURES AND ORBITALS ANALYSIS

The band structures and partial density of states (PDOS) of pristine monolayer MoS_2, $MoSe_2$, WS_2, and WSe_2 calculated by PBE are shown in Figs. 1(b)–1(e). All of the four TMDCs we considered here are direct band-gap semiconductors with both valence band maximum (VBM) and conduction band

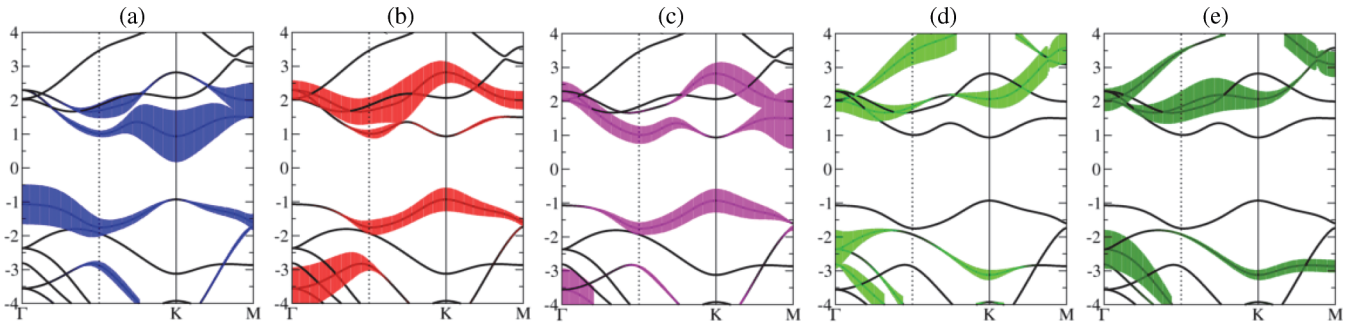

FIG. 2. (Color online) The band structure of pristine MoS_2 is orbitally resolved into (a) d_{z^2}, (b) $d_{x^2-y^2}$, (c) d_{xy}, (d) d_{xz}, and (e) d_{yz} orbitals. The vertical colored belt represents the strength of contributions.

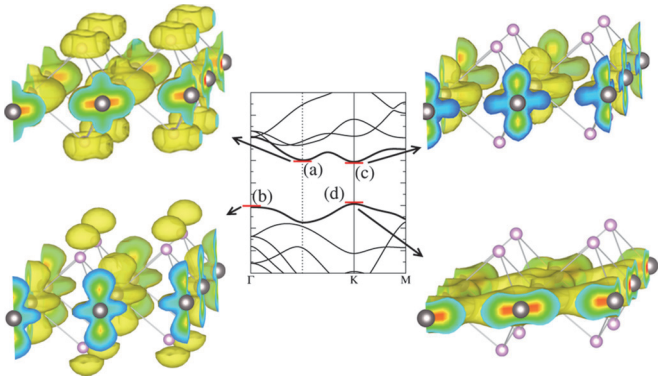

FIG. 3. (Color online) Charge densities on selected areas of CBM and VBM. From these charge densities, it is clear that (1) VBM at Γ [shown in (b)] and CBM at K [shown in (c)] are both dominated by d_{z^2}, (2) the orbital contributing to the local minimum point of lowest conduction band along the Γ to K direction [shown in (a)] exhibit strong in-plane orbitals (d_{xy} and $d_{x^2-y^2}$) characters with minor contribution from d_{z^2}, and (3) the characters of VBM at K are mostly d_{xy} and $d_{x^2-y^2}$ [shown in (d)]. Detailed contributions of each d orbital can be found in Fig. 2.

minimum (CBM) located at the K point of the first Brillouin zone. The values of their band gaps are summarized in Table I. By analyzing the PDOS, we can see that the electronic states near the CBM and VBM contributed mainly from d_{z^2} (blue), $d_{x^2-y^2}$ (red), and d_{xy} (red) orbitals of the M atom (Mo and W) and the p (black) orbitals of the X atom (S and Se). The strong coupling between p orbitals of the X atom and $d_{xz}+d_{yz}$ orbitals of the M atom leads to a large splitting between their bonding and antibonding states. Thus, d_{xz} and d_{yz} orbitals do not directly contribute to states near CBM and VBM as shown by the green PDOS in Fig. 1.

Noteworthily, for all four monolayer materials, there are local minima at the bottoms of the conduction bands alone the Γ to K direction. (For convenience, we refer to this point as the Λ point throughout the paper.) The energy of the conduction band at this Λ point is very close to that of global minimum at the K point. The two most extreme cases are $MoSe_2$ and WSe_2, where the gaps obtained with LDA turn indirect. To compare with available experimental results, where only direct gaps were reported, we thus show band structures calculated by PBE in the subsequent discussions. On the other hand, for low-dimensional systems, the strong exciton binding due to the weak screening of Coulomb interaction is considered important, thus, more sophisticated many-body methods, such as GW, are usually believed to provide better descriptions of electronic structures. It is, however, noted by several researchers that, for 2D MoS_2 and several other single-layer honeycomb structures,[20,31] band gaps predicted by LDA or PBE results agree better with experimental values than GW, although the physics behind it is not clear.

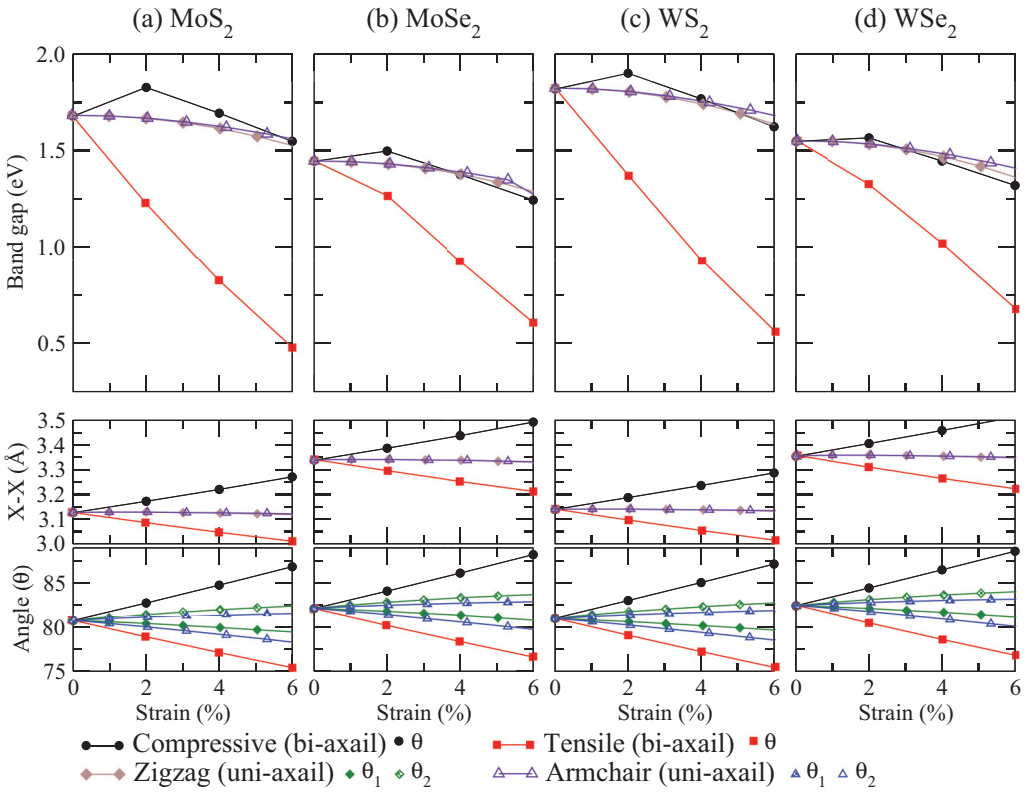

FIG. 4. (Color online) The dependence of band gaps of monolayer MX_2 calculated with PBE are shown in the upper panels. Evolutions of the X-X distance and X-M-X bond angle with respect to strains are plotted in the lower panels. Except within 2% of compressive biaxial strains, the band gaps are generally reduced as the strains increase. It is also clear that biaxial strains are more effective than the uniaxial strains in modulating the band gaps.

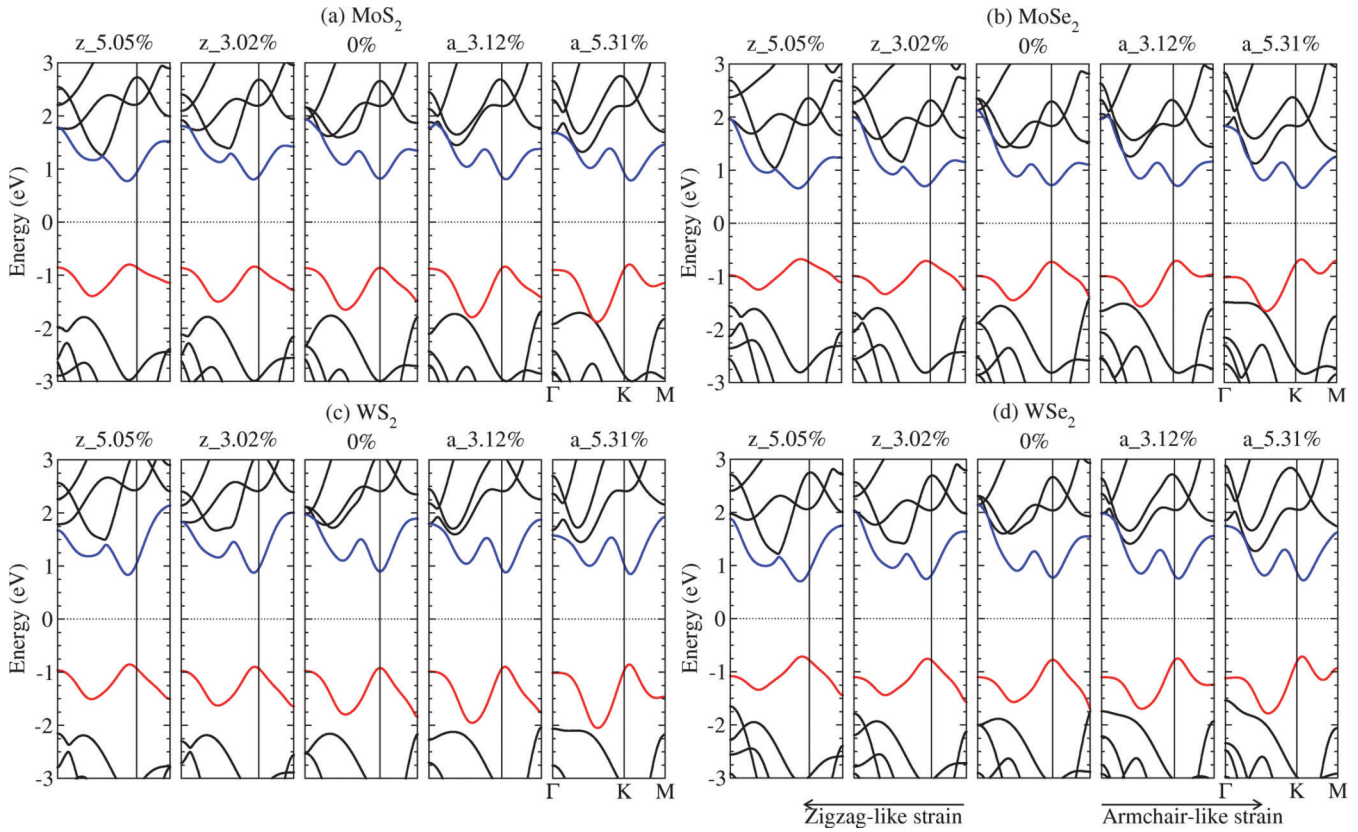

FIG. 5. (Color online) Change of band structures of MX_2 with uniaxial strains calculated by the PBE method. The lowest conduction band and highest valence band are highlighted in blue and red, respectively. Overall, the band structures are largely preserved, therefore, these monolayer MX_2 remain semiconductors with decreasing direct gaps. For comparison, the band structures of the pristine MX_2 are shown in the center. On the left-hand panels, under the zigzaglike strains, both CBM and VBM are shifted from the K point to a point between K-Γ. Under the armchairlike strains (shown on the right-hand panels), the CBM and VBM are shifted to between K-M.

To gain more physical insights on the interplay of the d orbitals, the band structure of pristine MoS_2 is orbitally resolved into d_{z^2}, $d_{x^2-y^2}$, d_{xy}, d_{xz}, and d_{yz} orbitals [shown in Figs. 2(a)–2(e), respectively] with the vertical colored belt representing the strengths of the contributions. As seen from Fig. 2(a), the highest valence band near the Γ point and the lowest conduction band near the K point have the contribution mainly from the d_{z^2} orbital. Both $d_{x^2-y^2}$ and d_{xy} orbitals share similar characters as shown in Figs. 2(b) and 2(c) and they dominate the states of the highest valence band near the K point and the states of lowest conduction band near the Λ point. Consistent with the interpretations from PDOS, d_{xz} [Fig. 2(d)] and d_{yz} [Fig. 2(e)] do not directly involve in the hybridization near VBM and CBM due to their stronger couplings with the p orbital of the X atom.

In Figs. 3(a)–3(d), we depict the spatial distribution of the charge density for selected points, discussed above, of the first Brillouin zone. It is obvious from Figs. 3(b) and 3(c) that the charge densities of the highest valence band near the Γ point and the lowest conduction band near the K points coincide with that of the d_{z^2} orbital. Meanwhile, the charge densities of the lowest conduction band near the Λ point [Fig. 3(a)] and the highest valence band near the K point [Fig. 3(d)] exhibit strong $d_{x^2-y^2}$ and d_{xy} characters. These spatial distributions provide consistent and complementary information with the analysis of the weight contributions of each d orbital on band structures shown in Fig. 2.

IV. CHANGE OF BAND STRUCTURES UNDER STRAINS

In general, structural relaxations under strains/stresses and changes in bond lengths/angles, would modulate the coupling strengths of the orbitals, resulting in the modulations of band gaps and phonon stiffness. For example, under compression the band gaps of most semiconductors are widened because the decreases in bond lengths typically strengthen the couplings and result in larger splittings between these orbitals. However, several theoretical papers have reported systematic reduction of band gaps of monolayer TMDCs under various strains.[16,18,32,33]

In this section, we examine the modulations of electronic band gaps under different strains. Accompanied with the orbital analysis in Sec. III, we further propose a mechanism which correlates the modulations to the structures and couplings between orbitals. The calculated band-gap evolutions (with PBE) under biaxial and uniaxial strains are shown in Fig. 4. Except within 2% of compressive biaxial strain, the band gap is generally reduced as the strain increases. Furthermore, it is also clear that biaxial strains are more effective than the uniaxial strains in modulating the band

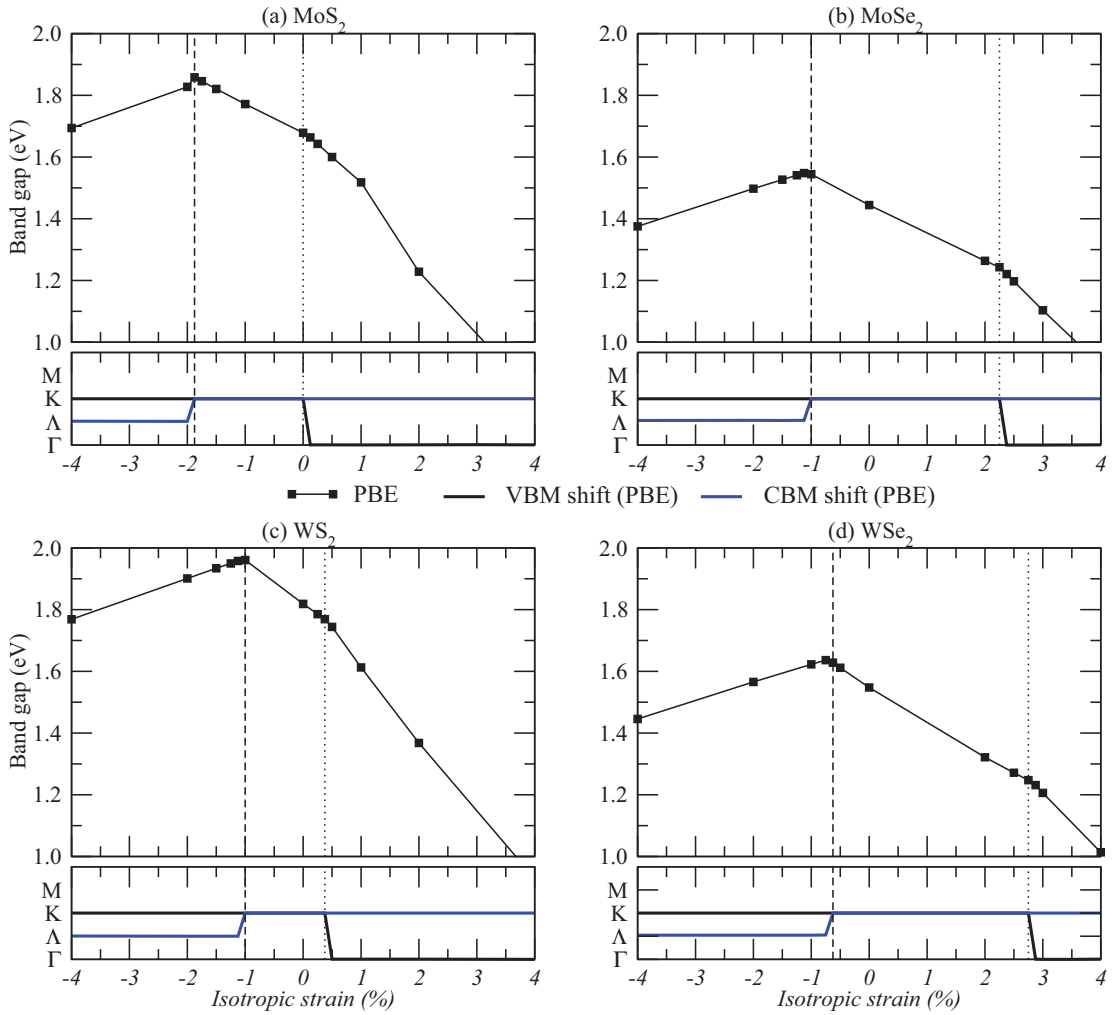

FIG. 6. (Color online) Band-gap variations of MX_2 with compressive and tensile biaxial strains are shown in the upper panel of each subfigure. The VBM (black line) and CBM (blue line) positions under strains are extracted in the lower panels. When the black and blue lines overlap, the gap is direct (VBM and CBM are at the same k point).

gaps. The change of the band structure can be correlated to a few key structural parameters. We depict the dependence of the X-M-X bond angle and X-X distance with respect to strains in the middle and lower panels in Fig. 4. It is obvious that these bond angles/lengths are more sensitive to biaxial strains. The essential difference in structural relaxations under biaxial and uniaxial strains can be attributed to the fact that under uniaxial strains, the quasi-2D lattice of TMDCs can relax along the out-of-plane directions leaving less change on these bond angles/lengths. We anticipate that the same notion can be generalized to other layered transition-metal oxides/chalcogenides. In the following, we detail the modulations under uniaxial and biaxial strains.

A. Uniaxial strains

We calculated band structures for various magnitudes of uniaxial strains, as shown in Fig. 5 (with lowest conduction band and highest valence band highlighted in blue and red, respectively). For each MX_2, the band structure of the pristine MX_2 is shown in the center. On the left-hand panels, under the zigzaglike strains, both CBM and VBM are shifted from the K point to a point between K-Γ. Under the armchairlike strains (shown on the right-hand panels), the CBM and VBM are shifted to between K-M. Up to 6% of uniaxial strains, the band structures are largely preserved and the monolayer MX_2 remains as a semiconductor with slightly decreasing direct band gaps.

Our results are consistent with previous works[16,33] and show that the reduction of band gaps under uniaxial strains is much smaller than biaxial ones. We further analyzed the structure parameters and proposed that the moderate change of band gaps under uniaxial strains can be correlated to the smoother changes of X-X distances and X-M-X angles. It is demonstrated in Fig. 4 that, even up to 6% of strains, X-X distances and X-M-X angles are only modified slightly, implying that the coupling strength between d_{z^2} and p orbitals is barely altered.

B. Biaxial strains

To be directly relevant to recent experimental results, a finer grid of applied strains is adopted to have a closer examination on changes of the band gaps within the experimental accessed

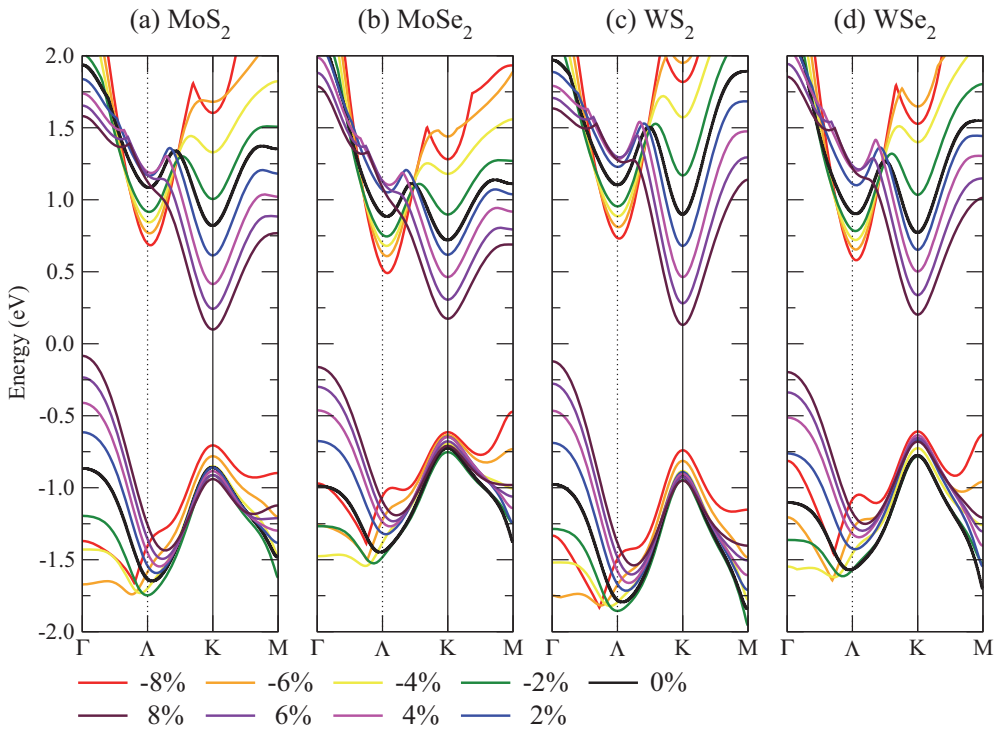

FIG. 7. (Color online) The change of highest valence band and lowest conduction band of MX_2 under compressive and tensile biaxial strains.

regime (±1%). The results of our finer grid calculations reveal different modulations of gaps from previous reports, where coarse grids were adopted.

Band gaps with various applied strains, both compressive and tensile, are shown in Fig. 6. The band-gap variations can be divided into three regimes: (1) In the central regime, monolayer MX_2 retains its direct band gap. Noteworthily, within 2% of compressive strains, it is possible to widen the direct band gaps by up to 10.7%, 7.8%, 6.9%, and 5.2% for MoS_2, WS_2, $MoSe_2$, and WSe_2. This finding is opposite to previous studies, which adopted coarse grids of applied strains and obtained reduction of gaps for all strains. (2) Exceeding these thresholds (shown as dashed lines), the compressive strains turn MX_2 into indirect semiconductors and the magnitudes of the band gap begin to decline. (3) If the tensile strains exceed the threshold on the right (shown as dotted lines), the band structures become indirect with much steeper slopes than the other two regimes. Our results detailed those band-gap widening/reducing transition regimes for sulfides and selenides and are consistent with recent studies on MoS_2 and WS_2,[15,19,21,34] where the emphases were laid on various regimes. The direct band-gap feature of selenides reported in this work was shown to be able to sustain even larger strains than sulfides (Fig. 6).

The dependence of the highest valence and lowest conduction bands under biaxial strains is shown in Fig. 7, demonstrating the band-gap evolution with strains. Under biaxial tensile strains, the X atom moves toward the M atom, which leads to a decrease in the X-M-X angle. Reduction of the X-M-X angle weakens the coupling between the p and d_{z^2} orbitals and strengthens coupling between the p and in-plane orbitals ($d_{x^2-y^2}$ and d_{xy}). Referring to the orbital analysis in Figs. 2 and 3, these modulations of couplings lead to (1) reduction of the gap between conduction band at the K point and valence band at the Γ point (due to d_{z^2} orbital) and (2) expansion of the gap between conduction band at the Λ point and valence band at the K point. As the intensity of tensile biaxial strains increases, eventually the valence bands at the Γ point become higher than those at the K point and the gaps turn indirect. Because the energy difference between valence bands at Γ and K points is large for MSe_2, MSe_2 can retain direct gaps for more than 2% of tensile strains. In MoS_2, however, the band gap can turn into indirect with small tensile strains, due to the near degeneracy of valence bands at the Γ and K points.

Application of compressive strains would increase the X-M-X bond angles. In contrast to tensile strains, the coupling between the p and d_{z^2} orbitals becomes stronger while the coupling between p orbital and in-plane orbitals ($d_{x^2-y^2}$ and d_{xy}) becomes weaker, thus modulating band structures in the opposite way. As the difference between the energies of conduction bands at the Λ and the K points is large, the direct gap of MoS_2 can be retained and even widened by 10.7%. Therefore, we showed that the direct band gaps of MX_2 can be robustly widened by applying compressive biaxial strains.

V. CHANGE OF PHONON DISPERSIONS UNDER STRAINS

Phonon propagation is determined by the bond strengths. Therefore, the X-M-X angle bending, and the resulting modulations of couplings between orbitals, not only alters the band structures as discussed in last section, but also the phonon stiffness.

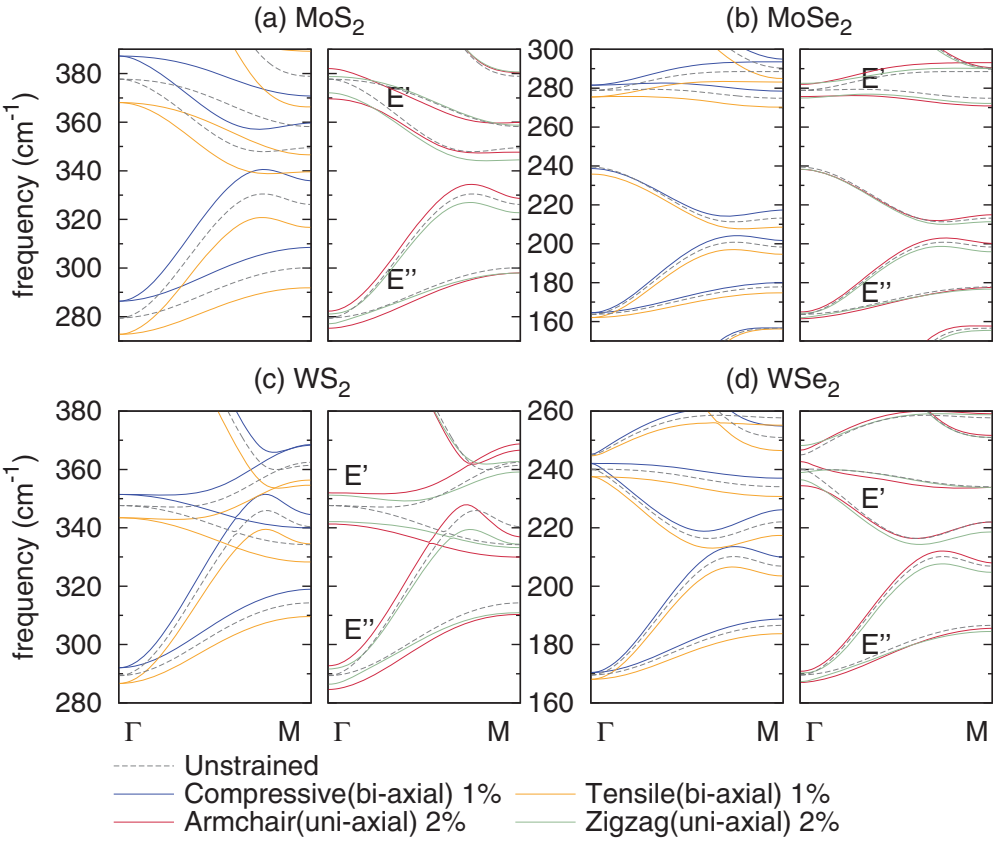

FIG. 8. (Color online) Phonon dispersions of MX_2. For compressive (tensile) bi-axial strains, the phonon frequencies are shifted upward (downward). For uniaxial strains, the degeneracies of E' and E'' phonon modes at Γ are lifted due to the introduced anisotropy of bond strengths.

With uniaxial strains, the changes in X-M-X angles, although moderate, can introduce the in-plane anisotropy of bond strengths. X-M-X angles are no longer isotropic under uniaxial strains but, instead, split into two different angles depending on their orientations with respect to the uniaxial strains (see Fig. 4, the split two angles are labeled with solid and hollow symbols). One of the two increases, while the other decreases with the increasing strains. From the orbital decompositions in Sec. III, it can be seen that the two types of X-M-X angles have opposite contributions to the coupling strengthening of the p and the in-plane d orbitals [one can refer to Figs. 2(b) and 2(c) for their contributions in band structures], hence generating the in-plane anisotropy.

The introduced anisotropy of bond strengths is further justified in the calculated phonon dispersion, as shown in Fig. 8. The degeneracies of in-plane E' and E'' phonon modes at Γ are lifted, and coincide with recent Raman spectroscopy results.[36] The generated splittings associated with 2% uniaxial armchair strains are 7.04 cm^{-1} (E'') and 12.44 cm^{-1} (E') for MoS_2, 3.48 cm^{-1} (E'') and 6.27 cm^{-1} (E') for $MoSe_2$, 8.12 cm^{-1} (E'') and 10.66 cm^{-1} (E') for WS_2, and 3.83 cm^{-1} (E'') and 8.27 cm^{-1} (E') for WSe_2. In the mean time, the average of the Raman shifts of the two split modes decreases with the increasing strains, also consistent with the observed Raman shifts. Our results can also be compared with the recent study on phonon shifts of large MoS_2 and WS_2 nanotubes,[35] which is similar to MX_2 with uniaxial strains. It was also suggested there that modifications of phonon modes can be utilized to monitor the electromechanical variations with Raman spectroscopy.

On the other hand, although there are greater changes in X-M-X angles for biaxial strained systems than uniaxial strained ones, there is however no anisotropy introduced. The modulations of bond strengths alter the phonon stiffness isotropically, and are demonstrated in the frequency shifts of the phonon dispersion, without the splitting as in the uniaxial cases (see Fig. 8). For compressive (tensile) biaxial strains, the phonon frequencies are shifted upward (downward). The harder (softer) phonon suggests stronger (weaker) bonding strength. Thus, according to our discussion in the end of the last section, it implies that the coupling most relevant to phonon propagations is the one between p orbitals of X atoms and d_{z^2} orbitals of M atoms. To be noted, aside from the structure relaxations (with Hellmann-Feynman forces acting on each atom less than 0.01 eV/Å), the stabilities of compressed MX_2 considered in this work are also confirmed by the full phonon dispersions, where the phonon frequencies are real across the the full dispersions when applying compressive strains. It is then of immediate relevance for the recent experimental advances in applying compressive strains.

VI. CONCLUSIONS

With first-principles calculations, we systematically investigate correlations among structures, orbital hybridizations,

band gaps, and phonon dispersions for monolayer MX_2 (M = Mo, W; X = S, Se) under biaxial and uniaxial strains. We found that the electronic structure near the band gap has the main contribution from d_{z^2} (out-of-plane) and $d_{x^2-y^2}$ and d_{xy} (in-plane) orbitals of M atoms and p orbitals of X atoms. Therefore, strains can effectively modulate the electronic structures and phonon dispersions through the change of the X-X distance and X-M-X bond angle. By comparison, biaxial strains are found to be more effective in tuning the band gap of monolayer MX_2 because MX_2 tends to be stretched more significantly along the out-of-plane direction resulting in greater changes in the bond lengths/angles. In addition, while most theoretical reports suggested systematic reduction of band gaps under mechanical strains, we found that the band gap can be widened by applying compressive biaxial strains. In MoS_2, for example, the direct gap can be widened by up to 10.7% with less than 2% of strain. On the other hand, the uniaxial strains can induce anisotropy of X-M-X bond angles and lead to splitting in the phonon dispersion, which is directly relevant to recent Raman spectroscopy results. As most TMDCs share the same structural characters, we expect that the notions derived here can open up new venues to engineer their optical and electronic properties for optoelectronic applications.

ACKNOWLEDGMENTS

This work was financially supported by the Academia Sinica Research Program on Nano Science and Nano Technology and the National Science Council (Grants No. NSC98-2113-M-001-029-MY3 and No. NSC101-2113-M-001-023-MY3) of Taiwan. Computational resources are supported in part by the National Center for High Performance Computing. C.-H.C. and S.-H. Lin would like to thank the support from the National Center for Theoretical Sciences (South) Physics Division. J-.L.K. would like to thank J. Li and X. Qian at MIT for useful comments and discussions during his visit.

*slin2@gate.sinica.edu.tw
†jlkuo@pub.iams.sinica.edu.tw

[1] K. S. Novoselov, D. Jiang, F. Schedin, T. J. Booth, V. V. Khotkevich, S. V. Morozov, and A. K. Geim, Proc. Natl. Acad. Sci. USA **102**, 10451 (2005).
[2] A. K. Geim and K. S. Novoselov, Nat. Mater. **6**, 183 (2007).
[3] K. S. Novoselov, A. K. Geim, S. Morozov, D. Jiang, Y. Zhang, S. Dubonos, I. Grigorieva, and A. Firsov, Science **306**, 666 (2004).
[4] M. Hamilton, L. Alvarez, N. Mauntler, N. Argibay, R. Colbert, D. Burris, C. Muratore, A. Voevodin, S. Perry, and W. G. Sawyer, Tribol. Lett. **32**, 91 (2008).
[5] B. Hinnemann, P. G. Moses, J. Bonde, K. P. Jorgensen, J. H. Nielsen, S. Horch, I. Chorkendorff, and J. K. Norskov, J. Am. Chem. Soc. **127**, 5308 (2005).
[6] H. D. Abrua, J. Electrochem. Soc. **129**, 2224 (1982).
[7] S. A. McDonald, G. Konstantatos, S. Zhang, P. W. Cyr, E. J. Klem, L. Levina, and E. H. Sargent, Nat. Mater. **4**, 138 (2005).
[8] Q. H. Wang, K. Kalantar-Zadeh, A. Kis, J. N. Coleman, and M. S. Strano, Nat. Nanotechnol. **7**, 699 (2012).
[9] K. F. Mak, C. Lee, J. Hone, J. Shan, and T. F. Heinz, Phys. Rev. Lett. **105**, 136805 (2010).
[10] A. Kuc, N. Zibouche, and T. Heine, Phys. Rev. B **83**, 245213 (2011).
[11] A. Kumar and P. K. Ahluwalia, Eur. Phys. J. B **85**, 186 (2012).
[12] A. Splendiani, L. Sun, Y. Zhang, T. Li, J. Kim, C. Y. Chim, G. Galli, and F. Wang, Nano Lett. **10**, 1271 (2010).
[13] A. Ramasubramaniam, Phys. Rev. B **86**, 115409 (2012).
[14] L. F. Mattheiss, Phys. Rev. B **8**, 3719 (1973).
[15] A. Sengupta, R. K. Ghosh, and S. Mahapatra, IEEE Trans. Electron Devices **60**, 2782 (2013).
[16] P. Johari and V. Shenoy, ACS Nano **6**, 5449 (2012).
[17] Y. Zhou, Z. Wang, P. Yang, X. Zu, L. Yang, X. Sun, and F. Gao, ACS Nano **6**, 9727 (2012).
[18] W. S. Yun, S. W. Han, S. C. Hong, I. G. Kim, and J. D. Lee, Phys. Rev. B **85**, 033305 (2012).
[19] S. Horzum, H. Sahin, S. Cahangirov, P. Cudazzo, A. Rubio, T. Serin, and F. M. Peeters, Phys. Rev. B **87**, 125415 (2013).
[20] H. Shi, H. Pan, Y. W. Zhang, and B. I. Yakobson, Phys. Rev. B **87**, 155304 (2013).
[21] T. Li, Phys. Rev. B **85**, 235407 (2012).
[22] P. E. Blöchl, Phys. Rev. B **50**, 17953 (1994).
[23] G. Kresse and D. Joubert, Phys. Rev. B **59**, 1758 (1999).
[24] G. Kresse and J. Hafner, Phys. Rev. B **48**, 13115 (1993).
[25] F. Fuchs, J. Furthmüller, F. Bechstedt, M. Shishkin, and G. Kresse, Phys. Rev. B **76**, 115109 (2007).
[26] J. P. Perdew, K. Burke, and M. Ernzerhof, Phys. Rev. Lett. **77**, 3865 (1996).
[27] S. Grimme, J. Comput. Chem. **27**, 1787 (2006).
[28] A. Togo, F. Oba, and I. Tanaka, Phys. Rev. B **78**, 134106 (2008).
[29] H. R. Gutieŕrez, N. Perea-López, A. L. Elias, A. Berkdemir, B. Wang, R. Lv, F. López-Urias, V. H. Crespi, H. Terrones, and M. Terrones, Nano Lett. **13**, 3447 (2013).
[30] P. Tonndorf, R. Schmidt, P. Boettger, X. Zhang, J. Boerner, A. Liebig, M. Albrecht, C. Kloc, O. Gordan, D. R. T. Zahn, S. M. Vasconcellos, and R. Bratschitsch, Opt. Express **21**, 4908 (2013).
[31] C. Ataca, H. Sahin, and S. Ciraci, J. Phys. Chem. C **116**, 8983 (2012).
[32] E. Scalise, M. Houssa, G. Pourtois, V. Afanas'ev, and A. Stesmans, Nano Res. **5**, 43 (2011).
[33] P. Lu, X. J. Wu, W. L. Guo, and X. C. Zeng, Phys. Chem. Chem. Phys. **14**, 13035 (2012).
[34] M. Ghorbani-Asl, S. Borini, A. Kuc, and T. Heine, Phys. Rev. B **87**, 235434 (2013).
[35] M. Ghorbani-Asl, N. Zibouche, M. Wahiduzzaman, A. F. Oliveira, A. Kuc, and T. Heine, Sci. Rep. **3**, 2961 (2013).
[36] H. Sahin, S. Tongay, S. Horzum, W. Fan, J. Zhou, J. Li, J. Wu, and F. M. Peeters, Phys. Rev. B **87**, 165409 (2013); H. J. Conley, B. Wang, J. I. Ziegler, R. F. Haglund, S. T. Pantelides, and K. I. Bolotin, Nano Lett. **13**, 3626 (2013); G. Wang, C. R. Zhu, B. L. Liu, X. Marie, Q. X. Feng, X. X. Wu, H. Fan, P. H. Tan, T. Amand, and B. Urbaszek, Phys. Rev. B **88**, 121301(R) (2013).